

## Supporting information

### Unsupported d<sup>8</sup>-d<sup>8</sup> interactions between dicationic Pd<sup>II</sup> and Pt<sup>II</sup> complexes: Evidence for a significant metal-metal bonding character

Jia Luo,<sup>a</sup> Julia R. Khusnutdinova,<sup>a</sup> Nigam P. Rath,<sup>b</sup> and Liviu M. Mirica<sup>a,\*</sup>

<sup>a</sup>Department of Chemistry, Washington University, St. Louis, Missouri, 63130-4899, U. S. A. Email: [mirica@wustl.edu](mailto:mirica@wustl.edu)

<sup>b</sup>Department of Chemistry and Biochemistry, University of Missouri – St. Louis, Missouri, 63121-4400, U. S. A.

#### Table of Contents

I. General experimental details	S2
II. Synthesis of the metal complexes	S3
III. ESI-MS spectra of 1 and 2	S6
IV. X-ray structure determinations of 1, 2 and 3	S8
V. <sup>1</sup> H Variable-temperature (VT) NMR studies of 1, 2 and 3	S14
VI. UV-vis spectra and Gaussian fits of 1, 2 and 3	S18
VII. Computational Details	S21
VIII. Reactivity studies of 3	S29
IX. References	S31

## I. General experimental details

### Reagents and materials

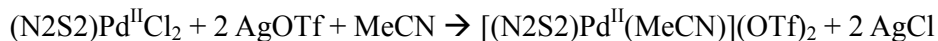
All chemicals were commercially available from Aldrich, Fisher or Strem Chemicals and were used as received without further purification. 2,11-dithia[3.3](2,6)pyridinophane (N2S2),<sup>1, 2</sup> Pd<sup>II</sup>Cl<sub>2</sub>(N2S2),<sup>2</sup> Pt<sup>II</sup>Cl<sub>2</sub>(N2S2),<sup>2</sup> and (COD)Pd<sup>II</sup>MeCl<sup>3</sup> were prepared according to the literature procedures. Solvents were purified prior to use by passing through a column of activated alumina using an MBraun solvent purification system.

### Physical measurements

<sup>1</sup>H (300.121 MHz) NMR spectra were recorded on a Varian Mercury-300 spectrometer. Variable temperature experiments were performed from 20 °C to -60 °C. Chemical shifts are reported in ppm and referenced to residual solvent resonance peaks. UV-vis spectra were recorded on a Varian Cary 50 Bio spectrophotometer. Solid-state UV-vis samples were prepared by mixing the finely ground powder with silicone oil (DC 200, Sigma-Aldrich) and pressed into a film on a glass coverslip. Gaussian fitting was performed using Peak functions-GaussAmp in the Origin 7.0 program. Elemental analyses were carried out by the Columbia Analytical Services Tucson Laboratory. ESI-MS experiments were performed on a Bruker Maxis Q-TOF mass spectrometer with an electron spray ionization source (ESI mass-spectrometry was provided by Washington University Mass Spectrometry Resource, a NIH Research Resource, grant No. P41RR0954).

## II. Syntheses of the metal complexes

### [Pd<sup>II</sup>(N2S2)(MeCN)]<sub>2</sub>(OTf)<sub>4</sub>, **1**



A solution of AgOTf (35.1 mg, 136.6 μmol) in MeCN (3 mL) was added to a stirred solution of Pd<sup>II</sup>Cl<sub>2</sub>(N2S2) (31.0 mg, 68.6 μmol) in MeCN (20 mL). A white precipitate of AgCl appeared immediately and the color of the solution changed from yellow to brown. Stirring was continued at room temperature for 2 h in the dark. The solvent was removed by rotary evaporation and the solid residue was redissolved in a minimum amount of MeCN. The resulting brown solution was filtered through Celite. The clear dark red filtrate was layered with anhydrous diethyl ether to give large dark-red crystals after several days at room temperature. Yield: 21.6 mg, 44%.

UV-vis (MeCN), λ, nm (ε, cm<sup>-1</sup> M<sup>-1</sup>): 515 (780), 342 (8120), 244 (28000).

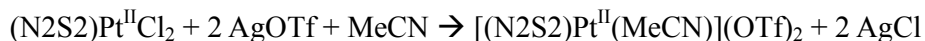
UV-vis (acetone), λ, nm (ε, cm<sup>-1</sup> M<sup>-1</sup>): 523 (1300), ~339 (19000).

<sup>1</sup>H NMR (CD<sub>3</sub>CN, 300 MHz), δ (ppm): 4.48 (d, *J* = 16.2 Hz, 4H, CH<sub>2</sub>), 5.08 (d, *J* = 16.2 Hz, 4H, CH<sub>2</sub>), 7.21 (d, *J* = 7.5 Hz, 4H, Py H<sub>meta</sub>), 7.59 (t, *J* = 7.5 Hz, 2H, Py H<sub>para</sub>).

Elemental analysis: found, C 30.05, H 2.78, N 5.59%; calculated C<sub>36</sub>H<sub>34</sub>F<sub>12</sub>N<sub>6</sub>O<sub>12</sub>Pd<sub>2</sub>S<sub>8</sub>, C 30.03, H 2.38, N 5.84%.

ESI-MS (*m/z*): 189.9811, calculated for [(N2S2)Pd<sup>II</sup>]<sup>2+</sup>: 189.9816; 528.9193, calculated for {(N2S2)Pd<sup>II</sup>}(OTf)<sup>+</sup>: 528.9153; 1058.8364, calculated for {(N2S2)Pd<sup>II</sup>]<sub>2</sub>(OTf)<sub>2</sub> - H<sup>+</sup>}<sup>+</sup>: 1058.8271; 1208.7983, calculated for {(N2S2)Pd<sup>II</sup>]<sub>2</sub>(OTf)<sub>3</sub>}<sup>+</sup>, 1208.7829.

### [Pt<sup>II</sup>(N2S2)(MeCN)]<sub>2</sub>(OTf)<sub>4</sub>, **2**



A solution of AgOTf (28.8 mg, 112.1 μmol) in MeCN (1 mL) was added to a stirred suspension of Pt<sup>II</sup>Cl<sub>2</sub>(N2S2) (29.8 mg, 55.1 μmol) in MeCN (10 mL). The solution became bright yellow immediately. After stirring for 2 h in dark at RT, the solution became cloudy. The solvent was removed by rotary evaporation and the resulting red solid was dissolved in a minimum amount of MeCN (1 – 2 mL) and the orange solution was filtered through Celite. The filtrate was set to crystallize by anhydrous diethyl ether vapor diffusion. Dark red crystals formed after several days. Yield: 24.3 mg,

Electronic Supporting Information (ESI) for Chemical Communications  
This journal is (c) The Royal Society of Chemistry 2011

---

54%.

UV-vis (MeCN),  $\lambda$ , nm ( $\epsilon$ ,  $\text{cm}^{-1} \text{M}^{-1}$ ): 404 (1290), 356 (3030), 260 (22000).

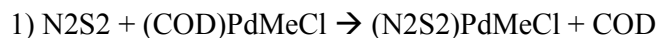
UV-vis (acetone),  $\lambda$ , nm ( $\epsilon$ ,  $\text{cm}^{-1} \text{M}^{-1}$ ): 410 (1180), ~345 (3500).

$^1\text{H}$  NMR ( $\text{CD}_3\text{CN}$ , 300 MHz),  $\delta$  (ppm): 4.72 (d,  $J = 16.2$  Hz, 4H,  $\text{CH}_2$ ), 5.14 (d,  $J = 16.2$  Hz, 4H,  $\text{CH}_2$ ), 7.27 (d,  $J = 7.5$  Hz, 4H, Py  $\text{H}_{\text{meta}}$ ), 7.60 (t,  $J = 7.5$  Hz, 2H, Py  $\text{H}_{\text{para}}$ ).

Elemental analysis: found, C 26.45, H 2.57, N 4.65%; calculated  $\text{C}_{36}\text{H}_{34}\text{F}_{12}\text{N}_6\text{O}_{12}\text{Pt}_2\text{S}_8\text{H}_2\text{O}$ , C 26.44, H 2.22, N 5.14%.

ESI-MS ( $m/z$ ): 234.5113, calculated for  $[\text{Pt}^{\text{II}}(\text{N}2\text{S}2)]^{2+}$ : 234.5123; 312.3461, calculated for  $\{[(\text{N}2\text{S}2)\text{Pt}^{\text{II}}]_2 - \text{H}^+\}^{3+}$ : 312.3465; 326.0217, calculated for  $\{[(\text{N}2\text{S}2)\text{Pt}^{\text{II}}(\text{MeCN})\text{Pt}^{\text{II}}(\text{N}2\text{S}2)] - \text{H}^+\}^{3+}$ : 326.0220; 617.9812, calculated for  $\{[\text{Pt}^{\text{II}}(\text{N}2\text{S}2)](\text{OTf})\}^+$ : 617.9766; 1275.9840, calculated for  $\{[(\text{N}2\text{S}2)\text{Pt}^{\text{II}}(\text{MeCN})\text{Pt}^{\text{II}}(\text{N}2\text{S}2)](\text{OTf})_2 - \text{H}^+\}^+$ : 1275.9698.

### **$[(\text{N}2\text{S}2)\text{Pd}^{\text{II}}\text{Me}]_2(\text{OTf})_4$ , **3****



$\text{N}2\text{S}2$  (85.0 mg, 0.310 mmol) and  $(\text{COD})\text{PdMeCl}$  (82.4 mg, 0.310 mmol) were stirred in 50 mL of dry diethyl ether under  $\text{N}_2$  for 1 day. The yellow precipitate was filtered off, washed with ether, pentane, and dried under vacuum. The yellow solid was used for the synthesis of  $[(\text{N}2\text{S}2)\text{PdMe}]_2(\text{OTf})_2$  (**3**) without further purification. Yield: 105 mg, 79%.

UV-vis ( $\text{CH}_2\text{Cl}_2$ ),  $\lambda$ , nm ( $\epsilon$ ,  $\text{cm}^{-1} \text{M}^{-1}$ ): 390 (sh, 700), 330 (sh, 1900).

$^1\text{H}$  NMR ( $\text{CDCl}_3$ , 300 MHz),  $\delta$  (ppm): 0.79 (s, 3H, PdMe), 4.13 (d,  $J = 14$  Hz, 2H,  $\text{CH}_2$ ), 4.23 (d,  $J = 14$  Hz, 2H,  $\text{CH}_2$ ), 5.99 (d,  $J = 14$  Hz, 2H,  $\text{CH}_2$ ), 6.21 (d,  $J = 14$  Hz, 2H,  $\text{CH}_2$ ), 7.05 (d,  $J = 7$  Hz, 2H, Py  $\text{H}_{\text{meta}}$ ), 7.16 (d,  $J = 7$  Hz, 2H, Py  $\text{H}_{\text{meta}}$ ), 7.51 (t,  $J = 7$  Hz, 1H, Py  $\text{H}_{\text{para}}$ ), 7.60 (t,  $J = 7$  Hz, 1H, Py  $\text{H}_{\text{para}}$ ).

ESI-MS ( $m/z$ ): 394.9897, calculated for  $[(\text{N}2\text{S}2)\text{Pd}^{\text{II}}\text{Me}]^+$ : 394.9868; 414.9341, calculated for  $[(\text{N}2\text{S}2)\text{Pd}^{\text{II}}\text{Cl}]^+$ : 414.9322.

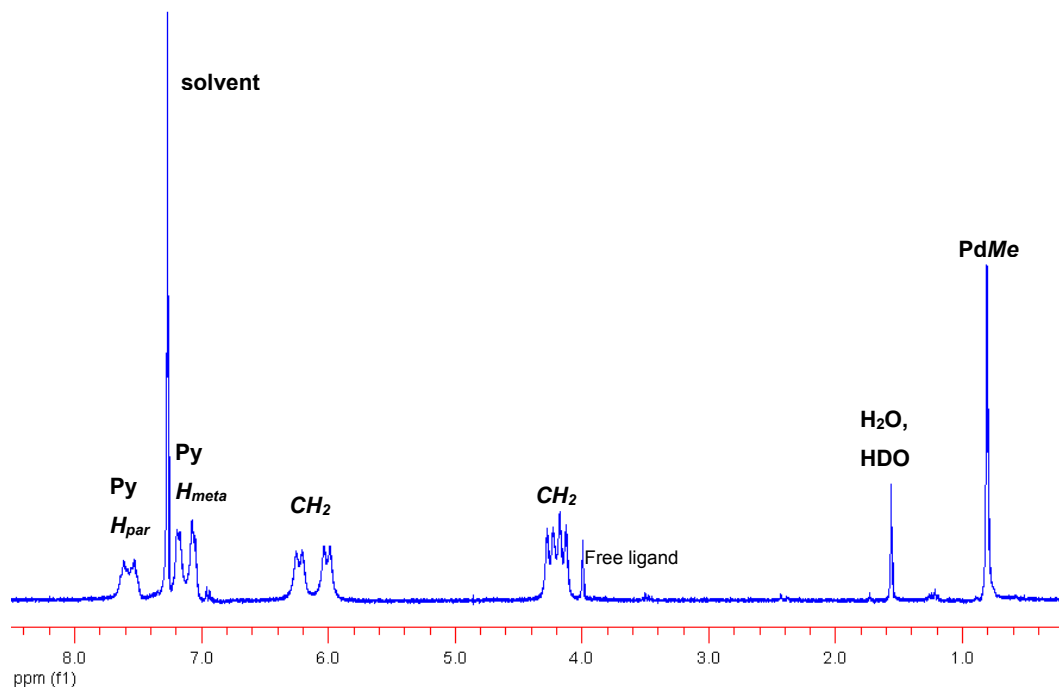
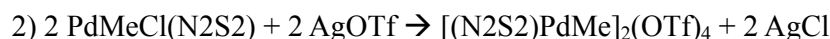


**Figure S1.**  $^1\text{H}$  NMR spectrum of  $(\text{N}_2\text{S}_2)\text{PdMeCl}$  in  $\text{CDCl}_3$ .



A solution of AgOTf (11.8 mg, 45.9  $\mu\text{mol}$ ) in acetone (1 mL) was added to a stirred suspension of  $(\text{N}_2\text{S}_2)\text{PdMeCl}$  (19.6 mg, 45.5  $\mu\text{mol}$ ) in acetone (10 mL). The solution became orange immediately. After stirring for 2~3 h in dark at RT under  $\text{N}_2$  flow, the solution became cloudy. The solvent was removed by rotary evaporation and the resulting orange-red solid was dissolved in a minimum amount of acetone (1 – 2 mL) and the orange solution was filtered through Celite. The filtrate was set to crystallize by ether diffusion. Dark red plates formed after several days at  $-20^\circ\text{C}$ . Yield: 24 mg, 100%.

UV-vis (MeCN),  $\lambda$ , nm ( $\epsilon$ ,  $\text{cm}^{-1} \text{M}^{-1}$ ): 346 (1400), 289 (4600).

UV-vis (acetone),  $\lambda$ , nm ( $\epsilon$ ,  $\text{cm}^{-1} \text{M}^{-1}$ ): 435 (390), ~340 (3800).

$^1\text{H}$  NMR (acetone- $d_6$ , 300 MHz),  $\delta$  (ppm): 1.00 (s, 3H,  $\text{CH}_3$ ), 4.75 (d,  $J = 15.8$  Hz, 4H,  $\text{CH}_2$ ), 4.88 (d,  $J = 15.8$  Hz, 4H,  $\text{CH}_2$ ), 7.24 (d,  $J = 7.6$  Hz, 4H, Py  $\text{H}_{\text{meta}}$ ), 7.50 (t,  $J = 7.6$  Hz, 2H, Py  $\text{H}_{\text{para}}$ ).

Elemental analysis: found, C 33.84, H 4.00, N 4.72%; calculated  $\text{C}_{32}\text{H}_{34}\text{F}_6\text{N}_4\text{O}_6\text{Pd}_2\text{S}_6 \cdot 3\text{H}_2\text{O}$ , C 33.60, H 3.52, N 4.90%.

ESI-MS ( $m/z$ ): 394.9903, calculated for  $[(\text{N}_2\text{S}_2)\text{Pd}^{\text{II}}\text{Me}]^+$ : 394.9868; 852.9628, calculated for  $\{[(\text{N}_2\text{S}_2)\text{Pd}^{\text{II}}\text{Me}]_2(\text{HCO}_3^-)\}^+$ : 852.9666.

### III. ESI-MS Spectra of 1 and 2

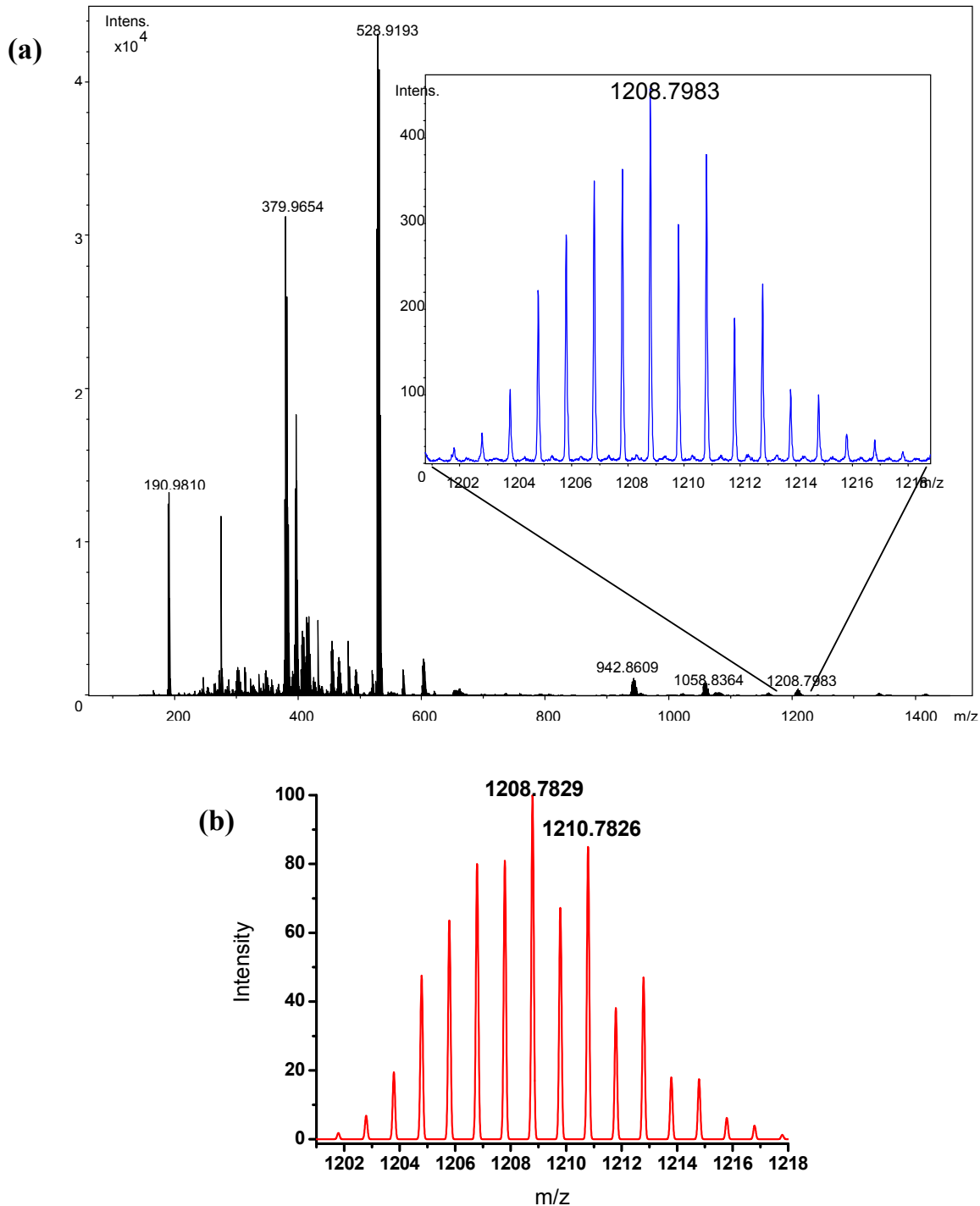


**Figure S2.** a) ESI-MS of the MeCN solution of **1**. Inset: the enlarged peak at 1208.7983, calculated for  $\{[(N2S2)Pd^{II}]_2(OTf)_3\}^+$ , 1208.7829. b) The simulation of the enlarged peak.

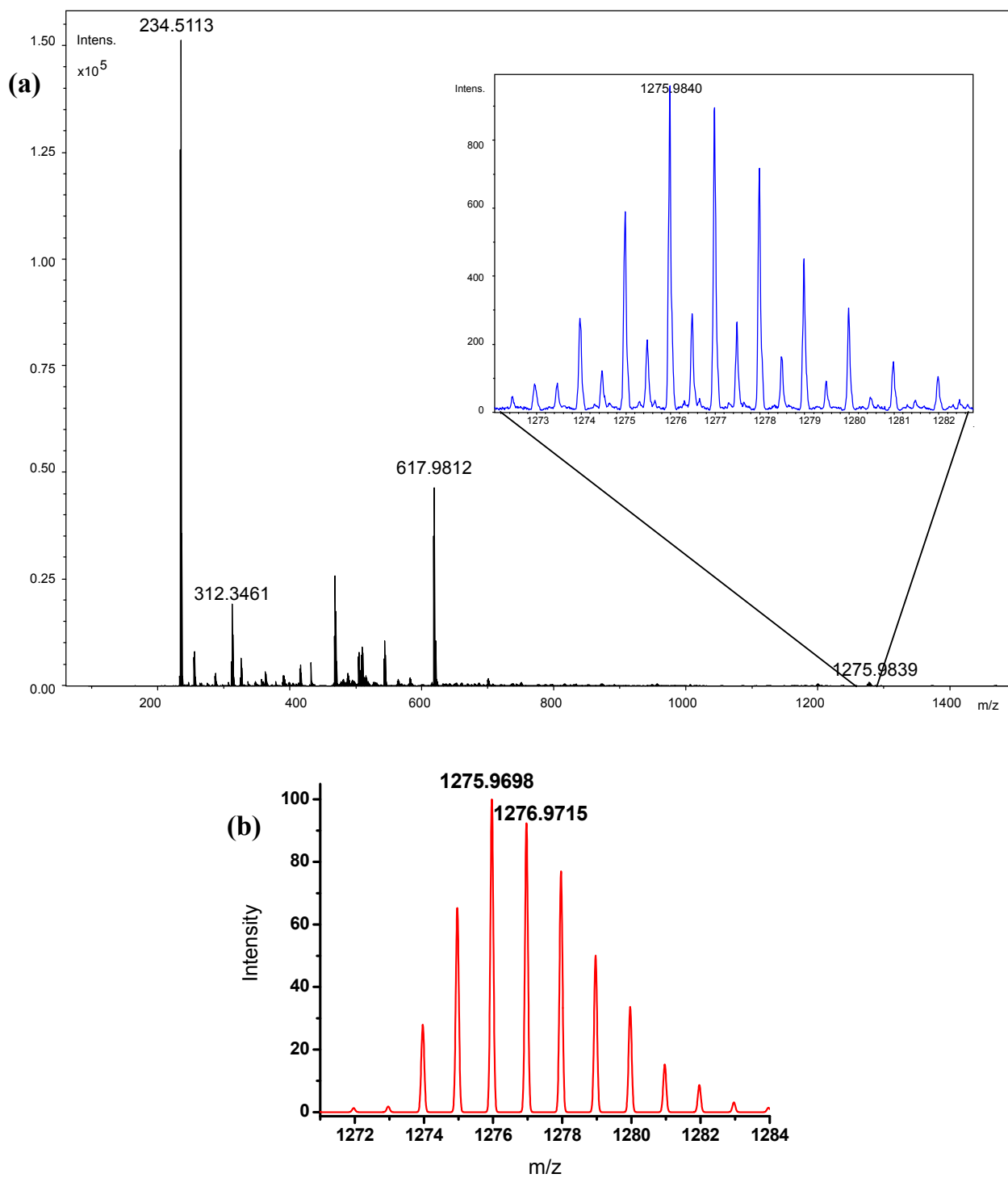


**Figure S3.** a) ESI-MS of the MeCN solution of **2**. Inset: the enlarged peak at 1275.9840, calculated for  $\{[(N_2S_2)Pt^{II}(MeCN)Pt^{II}(N_2S_2)](OTf)_2 - H^+\}^+$ : 1275.9698. b) The simulation of the enlarged peak.

#### IV. X-ray structure determinations of 1, 2 and 3

Crystals of X-ray diffraction quality were obtained by slow anhydrous diethyl ether vapor diffusion into acetonitrile or acetone solutions. Suitable crystals of appropriate dimensions were mounted on Mitgen loops in random orientations. Preliminary examination and data collection were performed using a Bruker Kappa Apex-II Charge Coupled Device (CCD) Detector system single crystal X-Ray diffractometer equipped with an Oxford Cryostream LT device. Data were collected using graphite monochromated Mo K $\alpha$  radiation ( $\lambda=0.71073$  Å) from a fine focus sealed tube X-Ray source. Preliminary unit cell constants were determined with a set of 36 narrow frame scans. Typical data sets consist of a combination of  $\omega$  and  $\phi$  scan frames with typical scan width of  $0.5^\circ$  and counting time of 15-30 seconds/frame at a crystal to detector distance of  $\sim 4.0$  cm. The collected frames were integrated using an orientation matrix determined from the narrow frame scans. Apex II and SAINT software packages (*Bruker Analytical X-Ray, Madison, WI, 2008*) were used for data collection and data integration. Analysis of the integrated data did not show any decay. Final cell constants were determined by global refinement of reflections from the complete data set. Data were corrected for systematic errors using SADABS (*Bruker Analytical X-Ray, Madison, WI, 2008*) based on the Laue symmetry using equivalent reflections. Funding from the National Science Foundation (MRI, CHE-0420497) for the purchase of the ApexII diffractometer is acknowledged.



Electronic Supporting Information (ESI) for Chemical Communications  
 This journal is (c) The Royal Society of Chemistry 2011

**Table S1.** Crystal data and structure refinement for **1**, **2** and **3**

Complex	<b>1</b>	<b>2</b>	<b>3</b>
Identification code	l23710.cif	l25810.cif	l4611.cif
Formula	C <sub>18</sub> H <sub>17</sub> F <sub>6</sub> N <sub>3</sub> O <sub>6</sub> Pd S <sub>4</sub>	C <sub>18</sub> H <sub>17</sub> F <sub>6</sub> N <sub>3</sub> O <sub>6</sub> Pt S <sub>4</sub>	C <sub>16</sub> H <sub>19</sub> F <sub>3</sub> N <sub>2</sub> O <sub>4</sub> Pd S <sub>3</sub>
<i>M</i>	719.99	808.68	562.91
System	Monoclinic	Monoclinic	Triclinic
Space group	P2 <sub>1</sub> /c	P2 <sub>1</sub> /c	P-1
a (Å)	12.3492(5)	12.3114(7)	9.7020(6)
b (Å)	17.5047(6)	17.5704(10)	10.3167(7)
c (Å)	12.1940(5)	12.2608(7)	10.6734(7)
α (°)	90.	90.	79.150(2)
β (°)	112.870(2)	112.402(3)	89.371(3)
γ (°)	90.	90.	75.100(3)
V (Å <sup>3</sup> )	2448.67(16)	2452.1(2)	1013.16(11)
Z	4	4	2
d <sub>calcd</sub> (Mg/m <sup>3</sup> )	1.953	2.191	1.845
Crystal size (mm <sup>3</sup> )	0.29 x 0.26 x 0.17	0.14 x 0.08 x 0.06	0.34 x 0.22 x 0.14
<i>T</i> (K)	100 (2)	100(2)	100(2)
λ (Å)	0.71073	0.71073	0.71073
μ (mm <sup>-1</sup> )	1.187	6.151	1.278
Independent reflections	10171	5083	15753
R(int)	0.0302	0.0696	0.0256
Collected reflections	52737	72537	74401
[I>2σ(I)] R1, wR2	0.0323, 0.0816	0.0241, 0.0464	0.0241, 0.0561

Electronic Supporting Information (ESI) for Chemical Communications  
 This journal is (c) The Royal Society of Chemistry 2011

**Table S2.** Selected bond lengths (Å) and selected bond angles (°) for **1**, **2** and **3**

	<b>1</b>		<b>2</b>		<b>3</b>
<i>Distances</i>					
Pd(1)-S(1)	2.3275(5)	Pt(1)-S(1)	2.3157(10)	Pd(1)-C(1)	2.0389(8)
Pd(1)-S(2)	2.3230(5)	Pt(1)-S(2)	2.3187(10)	Pd(1)-N(1)	2.1049(6)
Pd(1)-N(1)	2.0004(14)	Pt(1)-N(1)	2.005(3)	Pd(1)-S(2)	2.3370(2)
Pd(1)-N(2)	2.5054(16)	Pt(2)-N(2)	2.584(3)	Pd(1)-S(1)	2.3447(3)
Pd(1)-N(3)	2.0146(16)	Pt(1)-N(3)	1.995(3)	Pd(1)-N(2)	2.5739(7)
Pd(1)-Pd(1)'	3.0657(3)	Pt(1)-Pt(1)'	3.0768(3)	Pd(1)-Pd(1)'	3.1132(2)
<i>Angles</i>					
N(1)-Pd(1)-N(3)	179.14(6)	N(3)-Pt(1)-N(1)	178.80(12)	C(1)-Pd(1)-N(1)	175.25(3)
N(1)-Pd(1)-S(2)	86.13(4)	N(3)-Pt(1)-S(1)	93.65(10)	C(1)-Pd(1)-S(2)	95.17(3)
N(3)-Pd(1)-S(2)	93.71(5)	N(1)-Pt(1)-S(1)	86.25(9)	N(1)-Pd(1)-S(2)	84.563(19)
N(1)-Pd(1)-S(1)	85.59(4)	N(3)-Pt(1)-S(2)	94.27(10)	C(1)-Pd(1)-S(1)	94.04(3)
N(3)-Pd(1)-S(1)	94.35(5)	N(1)-Pt(1)-S(2)	85.48(9)	N(1)-Pd(1)-S(1)	84.68(2)
S(2)-Pd(1)-S(1)	163.060(18)	S(1)-Pt(1)-S(2)	161.57(4)	S(2)-Pd(1)-S(1)	158.629(8)
N(1)-Pd(1)-N(2)	84.87(5)	N(3)-Pt(1)-N(2)	93.99(11)	C(1)-Pd(1)-N(2)	92.93(3)
N(3)-Pd(1)-N(2)	94.27(6)	N(1)-Pt(1)-N(2)	84.81(10)	N(1)-Pd(1)-N(2)	82.34(2)
S(2)-Pd(1)-N(2)	82.38(4)	S(1)-Pt(1)-N(2)	81.50(8)	S(2)-Pd(1)-N(2)	80.448(16)
S(1)-Pd(1)-N(2)	82.19(4)	S(2)-Pt(1)-N(2)	81.37(8)	S(1)-Pd(1)-N(2)	79.854(16)
N(1)-Pd(1)-Pd(1)'	91.29(4)	N(3)-Pt(1)-Pt(1)'	91.17(9)	C(1)-Pd(1)-Pd(1)'	97.41(3)
N(3)-Pd(1)-Pd(1)'	89.57(4)	N(1)-Pt(1)-Pt(1)'	90.03(8)	N(1)-Pd(1)-Pd(1)'	87.266(18)
S(2)-Pd(1)-Pd(1)'	96.831(14)	S(1)-Pt(1)-Pt(1)'	97.87(3)	S(2)-Pd(1)-Pd(1)'	103.129(7)
S(1)-Pd(1)-Pd(1)'	98.103(14)	S(2)-Pt(1)-Pt(1)'	98.58(3)	S(1)-Pd(1)-Pd(1)'	94.741(7)
N(2)-Pd(1)-Pd(1)'	176.12(4)	N(2)-Pt(1)-Pt(1)'	174.83(7)	N(2)-Pd(1)-Pd(1)'	168.666(15)

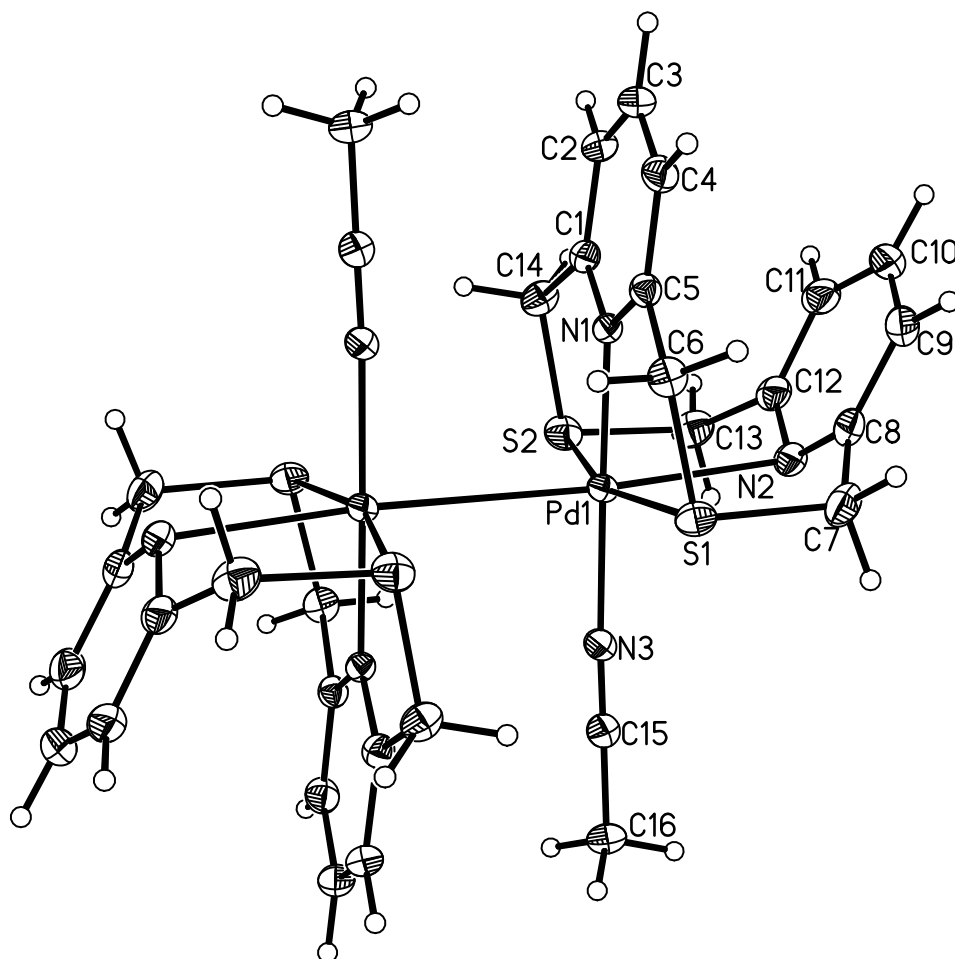


**Figure S4.** Projection view of  $[(N_2S_2)Pd(MeCN)]_2(OTf)_4$  (**1**) with 50% thermal ellipsoids. Triflate anions are omitted.

**Note:** In the extended crystal lattice structure of **1**, the shortest intermolecular pyridine ring centroid-centroid interplanar distance is 4.054 Å, suggesting a very weak, negligible  $\pi$ - $\pi$  stacking interaction.

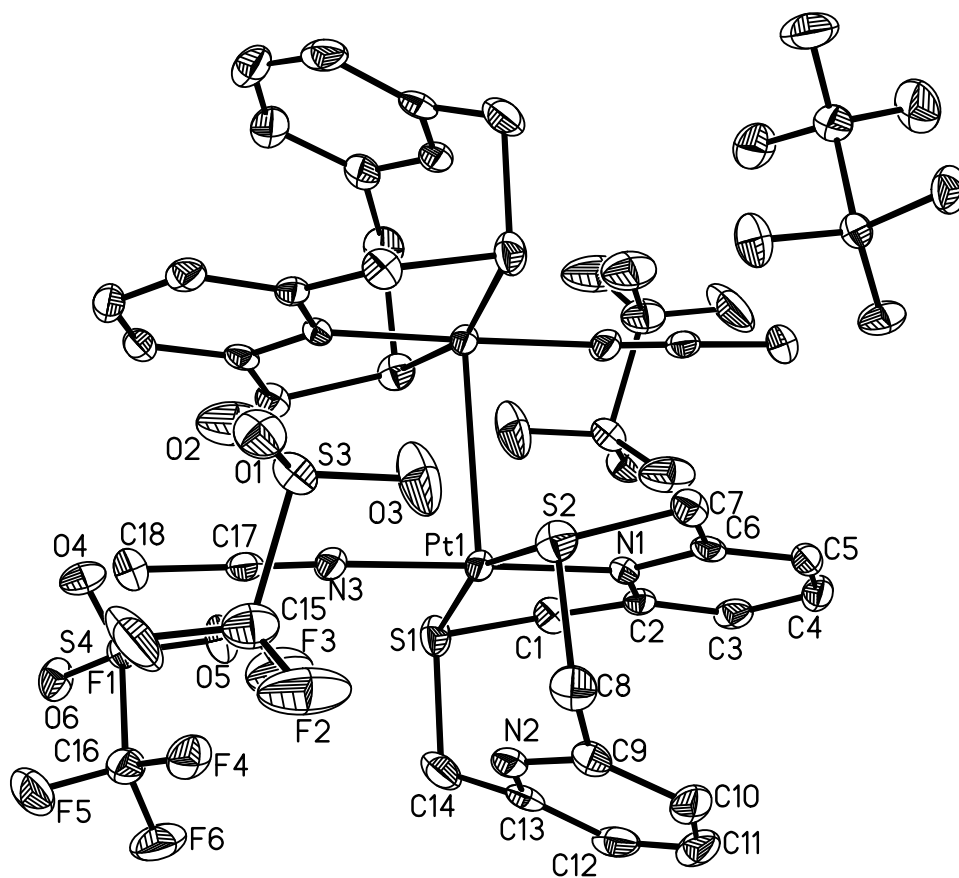


**Figure S5.** Projection view of  $[(N_2S_2)Pt(MeCN)]_2(OTf)_4$  (**2**) with 50% thermal ellipsoids. H atoms and disorder atoms are omitted for clarity.

**Note:** In the extended crystal lattice structure of **2**, the shortest intermolecular pyridine ring centroid-centroid interplanar distance is 4.170 Å, suggesting a very weak, negligible  $\pi$ - $\pi$  stacking interaction.

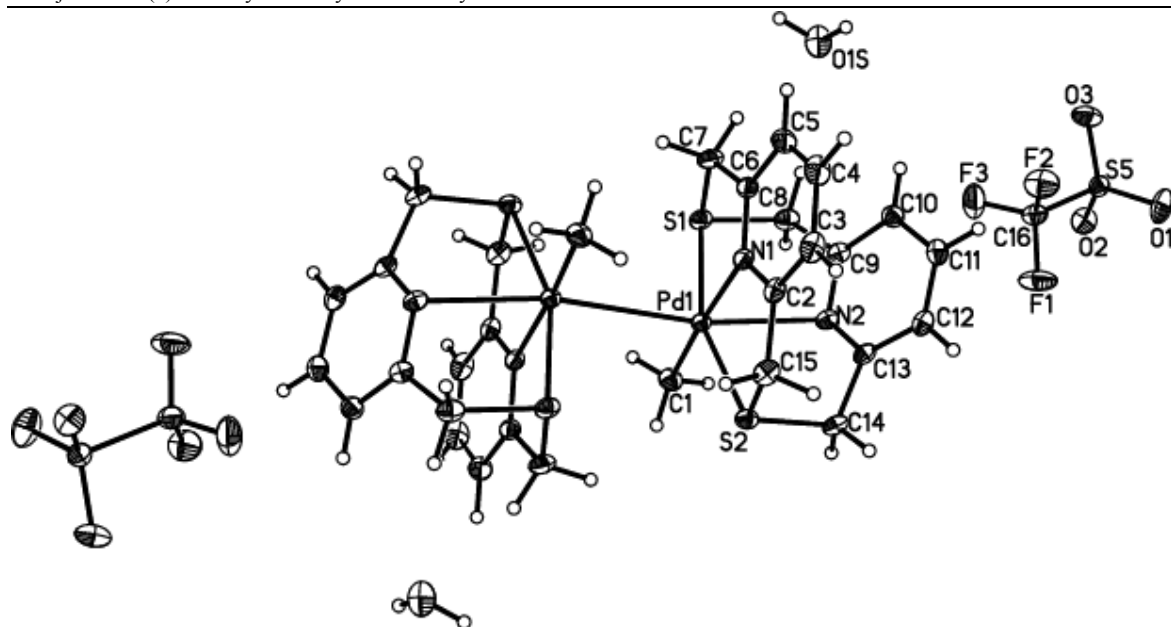


**Figure S6.** Projection view of  $[(N_2S_2)PdMe]_2(OTf)_2$  (**3**) with 50% thermal ellipsoids.

**Note:** For **3**, the axial pyridine ring is tilted at an angle of  $57.1^\circ$  vs the M-N2(py) bond and the centroid-centroid interplanar distance between the two pyridine rings of one N<sub>2</sub>S<sub>2</sub> ligand is 3.498 Å.

**Note:** No intermolecular pyridine ring  $\pi$ - $\pi$  stacking interaction exists in the extended crystal lattice of **3**.

Electronic Supporting Information (ESI) for Chemical Communications  
This journal is (c) The Royal Society of Chemistry 2011

## V. $^1\text{H}$ Variable-temperature (VT) NMR studies of 1, 2 and 3

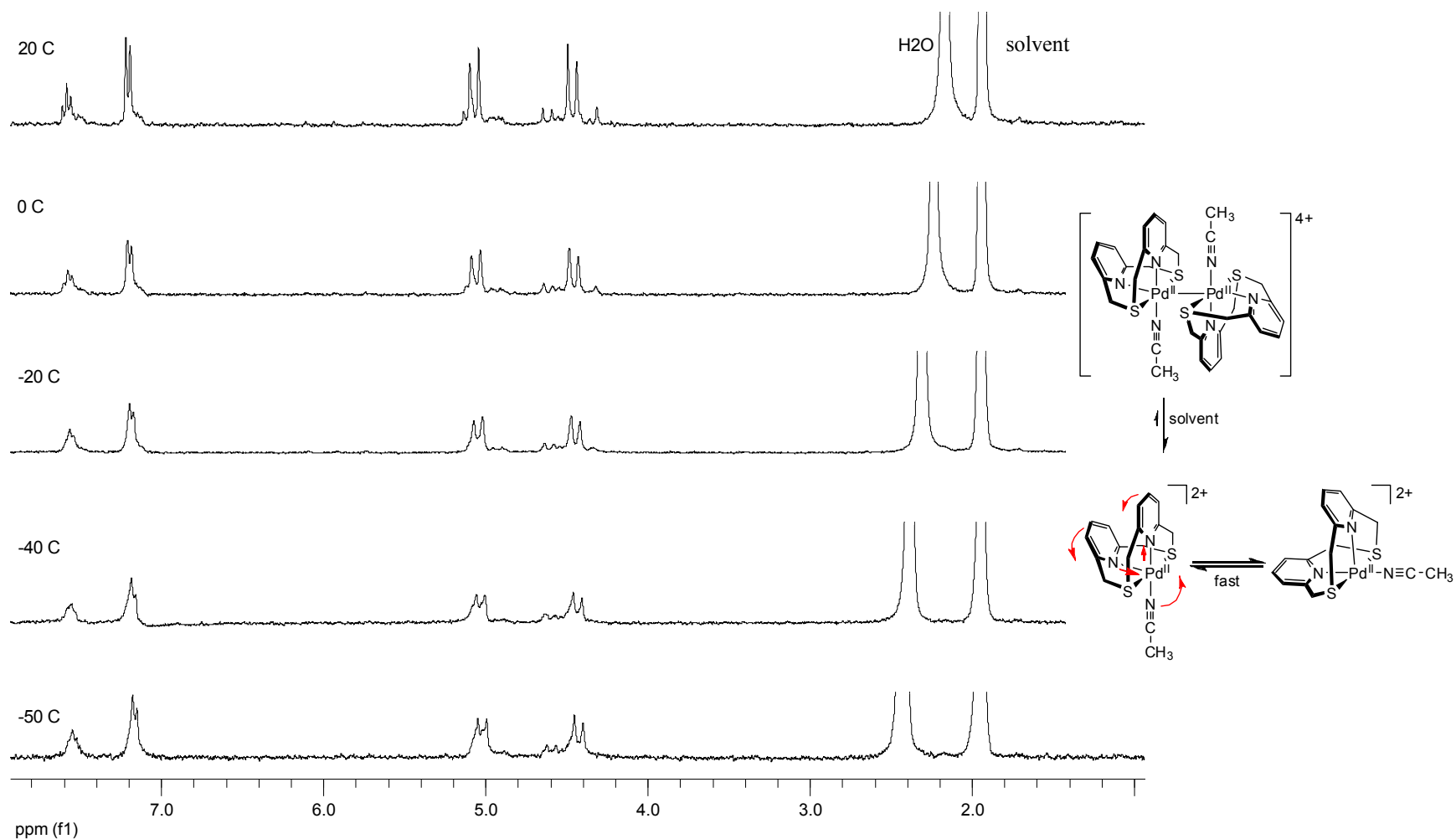


**Figure S7.**  $^1\text{H}$  VT NMR of **1** in  $\text{CD}_3\text{CN}$ . Left: Proposed fast ligand rearrangement for **1**. (Note: The spectrum of **1** in acetone- $d_6$  exhibits a similar behavior, although the NMR spectrum is complicated by the formation of more than one Pd-solvento complex).

Electronic Supporting Information (ESI) for Chemical Communications  
This journal is (c) The Royal Society of Chemistry 2011

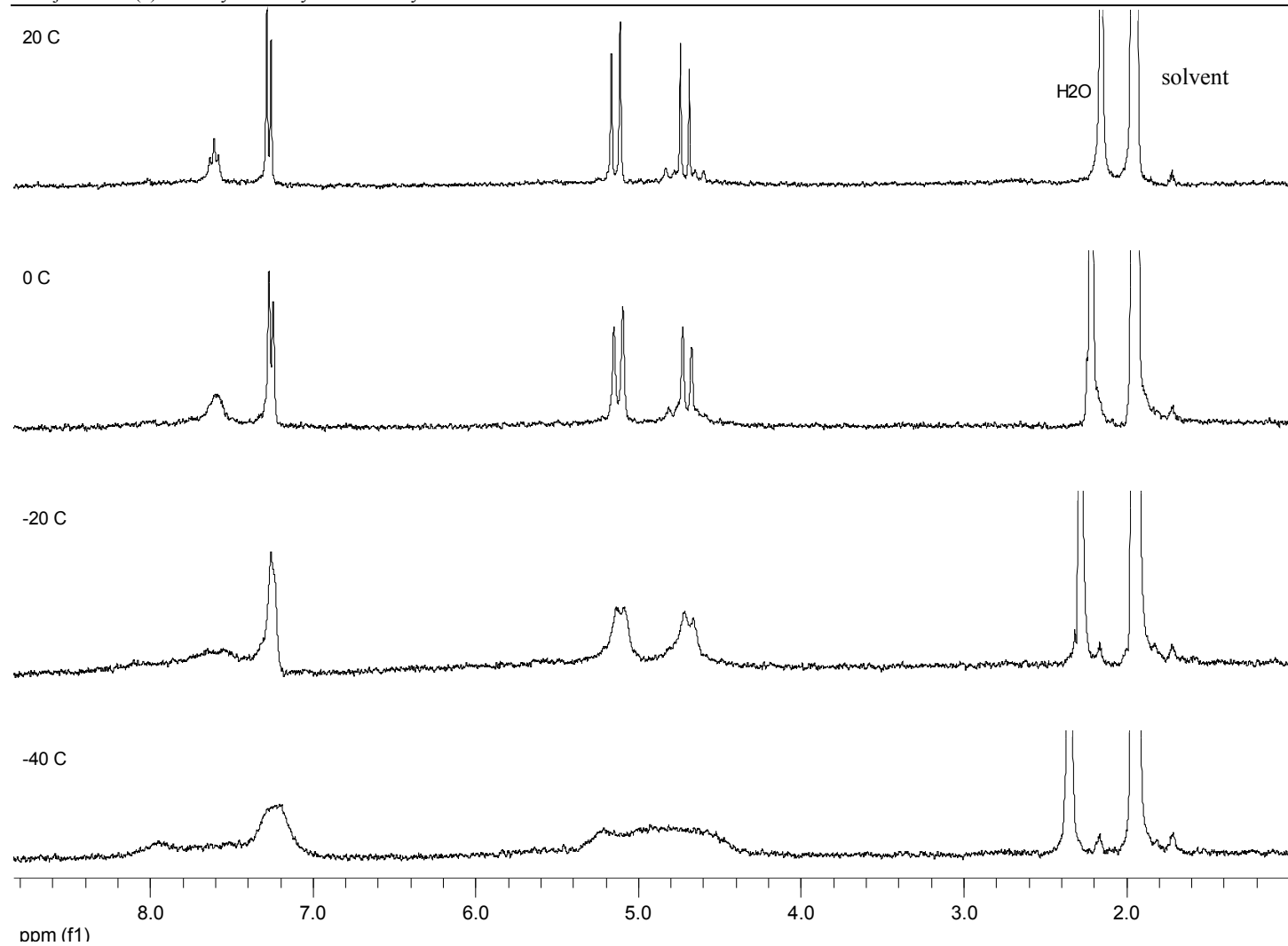


**Figure S8.**  $^1\text{H}$  VT NMR of **2** in  $\text{CD}_3\text{CN}$ .

Electronic Supporting Information (ESI) for Chemical Communications  
This journal is (c) The Royal Society of Chemistry 2011

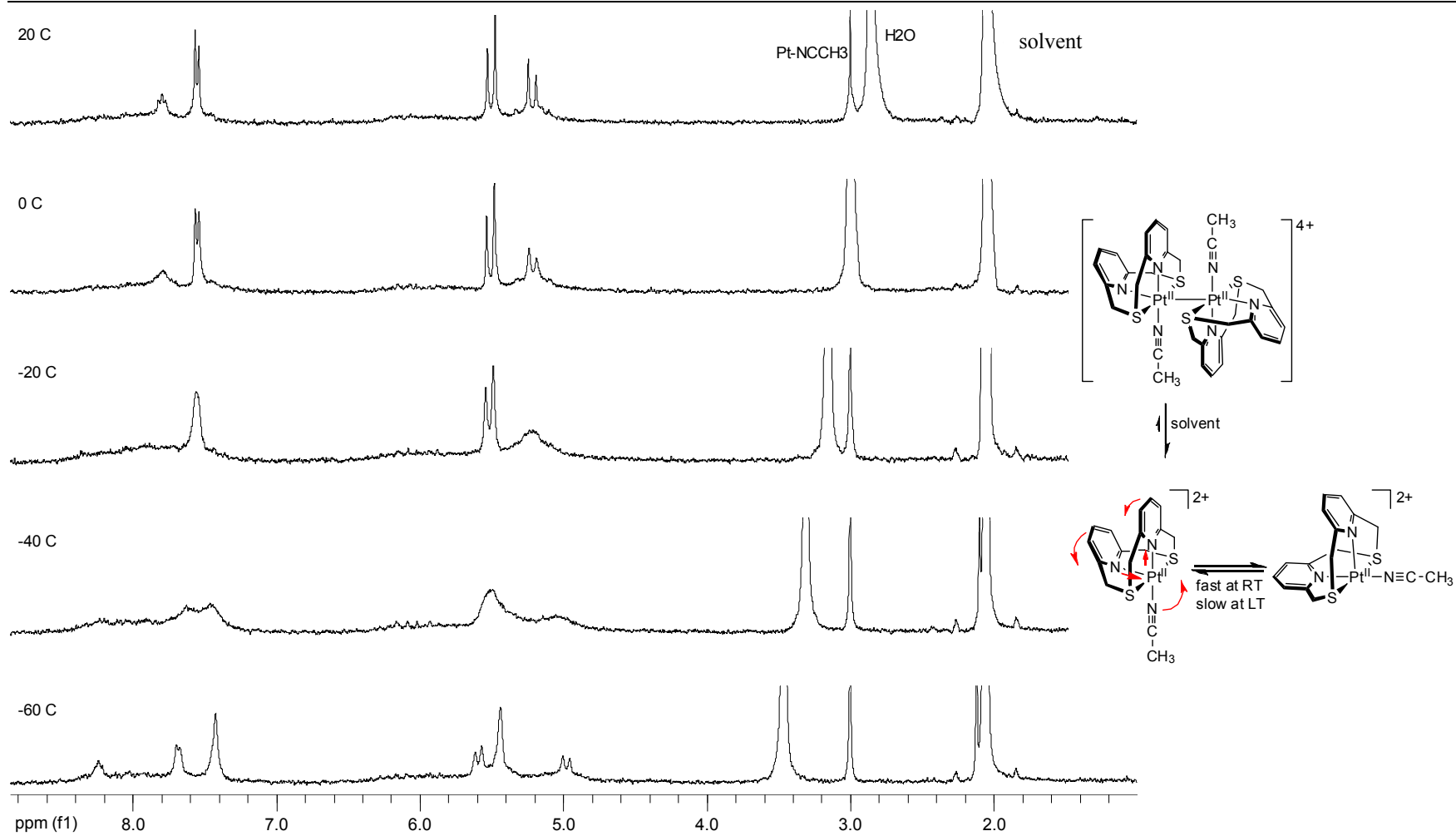


**Figure S9.**  $^1\text{H}$  VT NMR of **2** in acetone- $d_6$ . Left: Proposed fast ligand rearrangement occurring at room temperature for **2**.



Electronic Supporting Information (ESI) for Chemical Communications  
This journal is (c) The Royal Society of Chemistry 2011

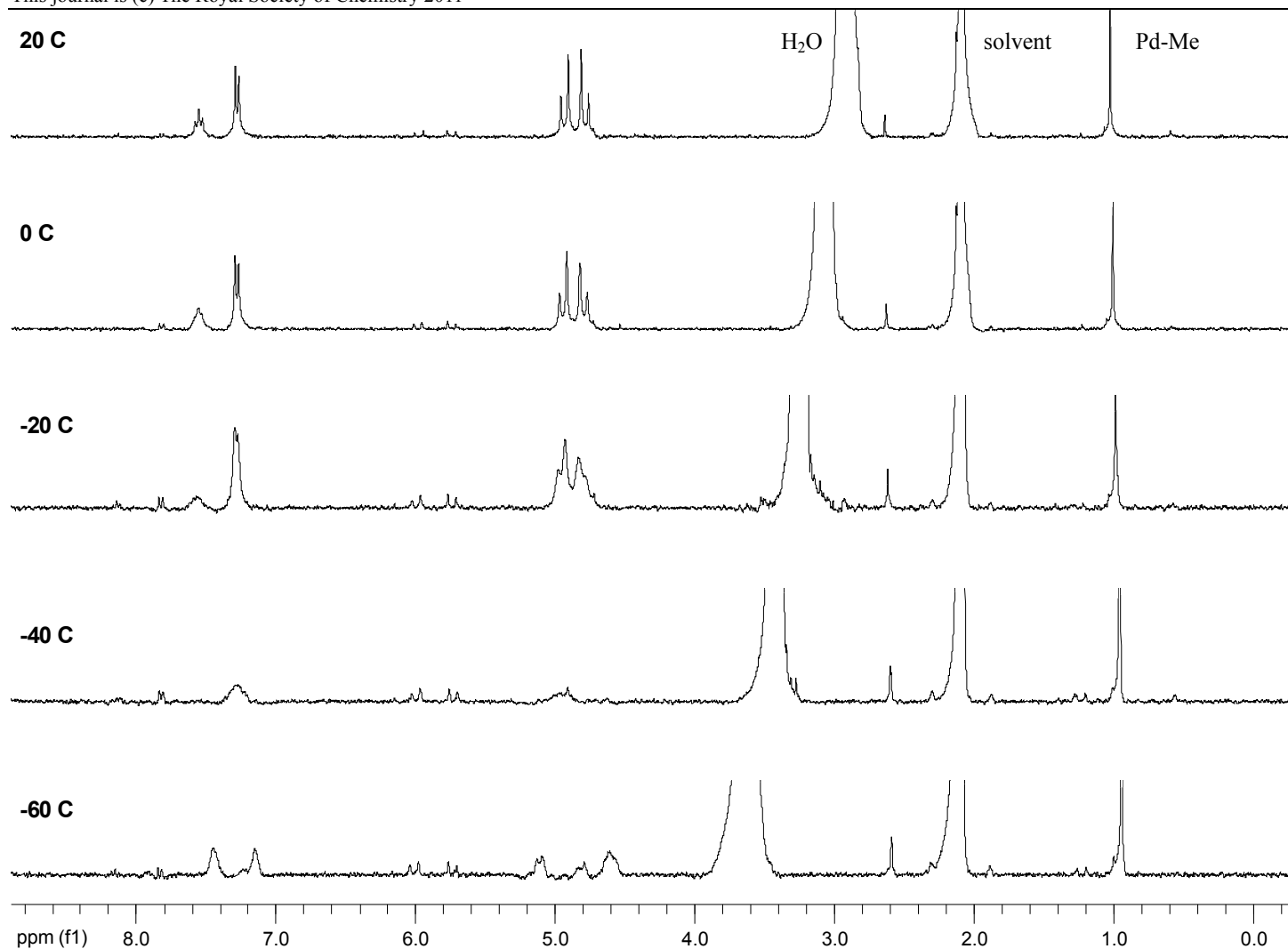


**Figure S10.**  $^1\text{H}$  VT NMR of **3** in acetone- $d_6$ . The small peaks around 6 ppm and 2.6 ppm are due to the  $[(\text{N}2\text{S}2)\text{Pd}^{\text{IV}}\text{Me}_2]^{2+}$  species, which is an oxidation byproduct from the synthesis of **3**.

## VI. UV-vis spectra and Gaussian fits of 1, 2 and 3

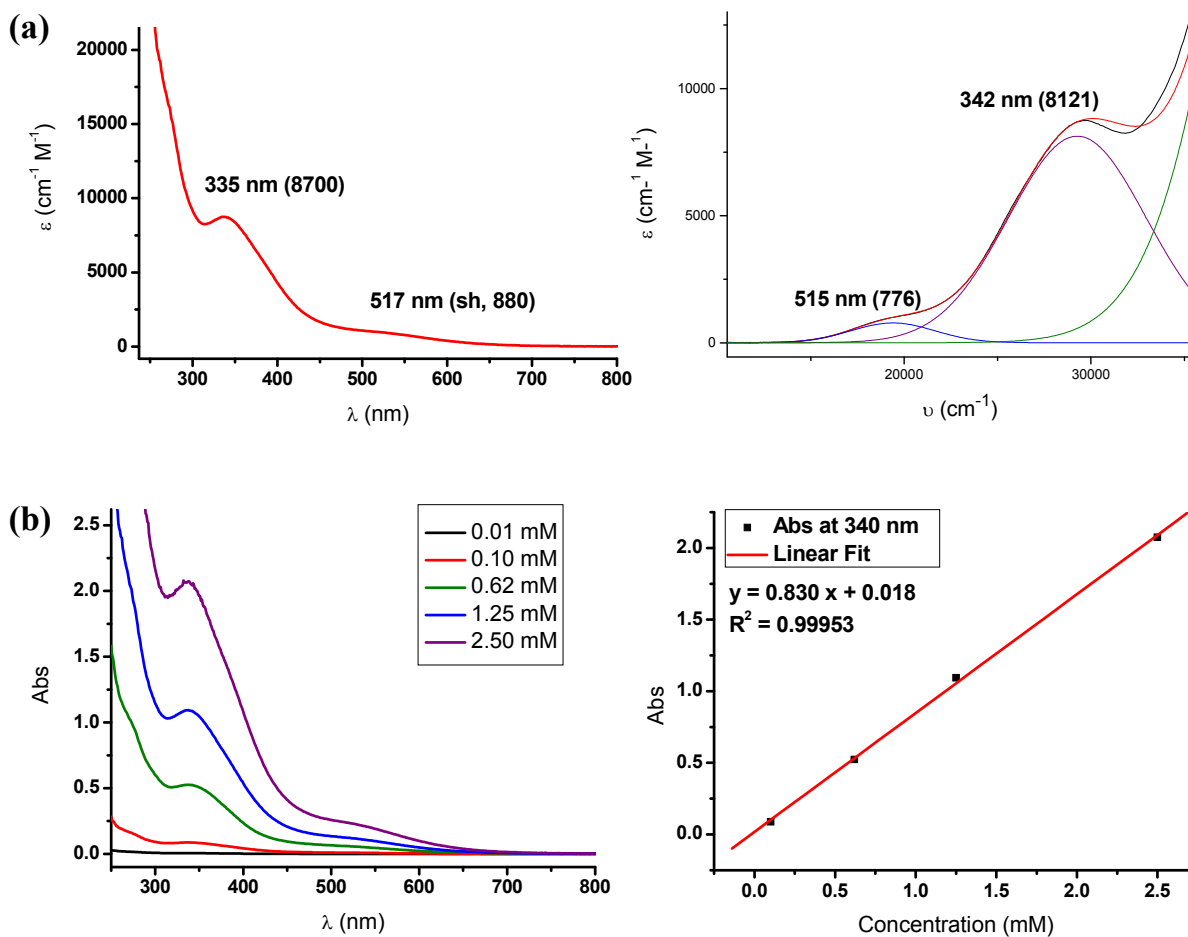


**Figure S11.** (a) UV-vis spectrum and Gaussian fit of **1** in MeCN; (b) overlay of UV-vis spectra at different concentrations (pathlength = 1.0 mm) and linear fit of the absorbance at 340 nm.

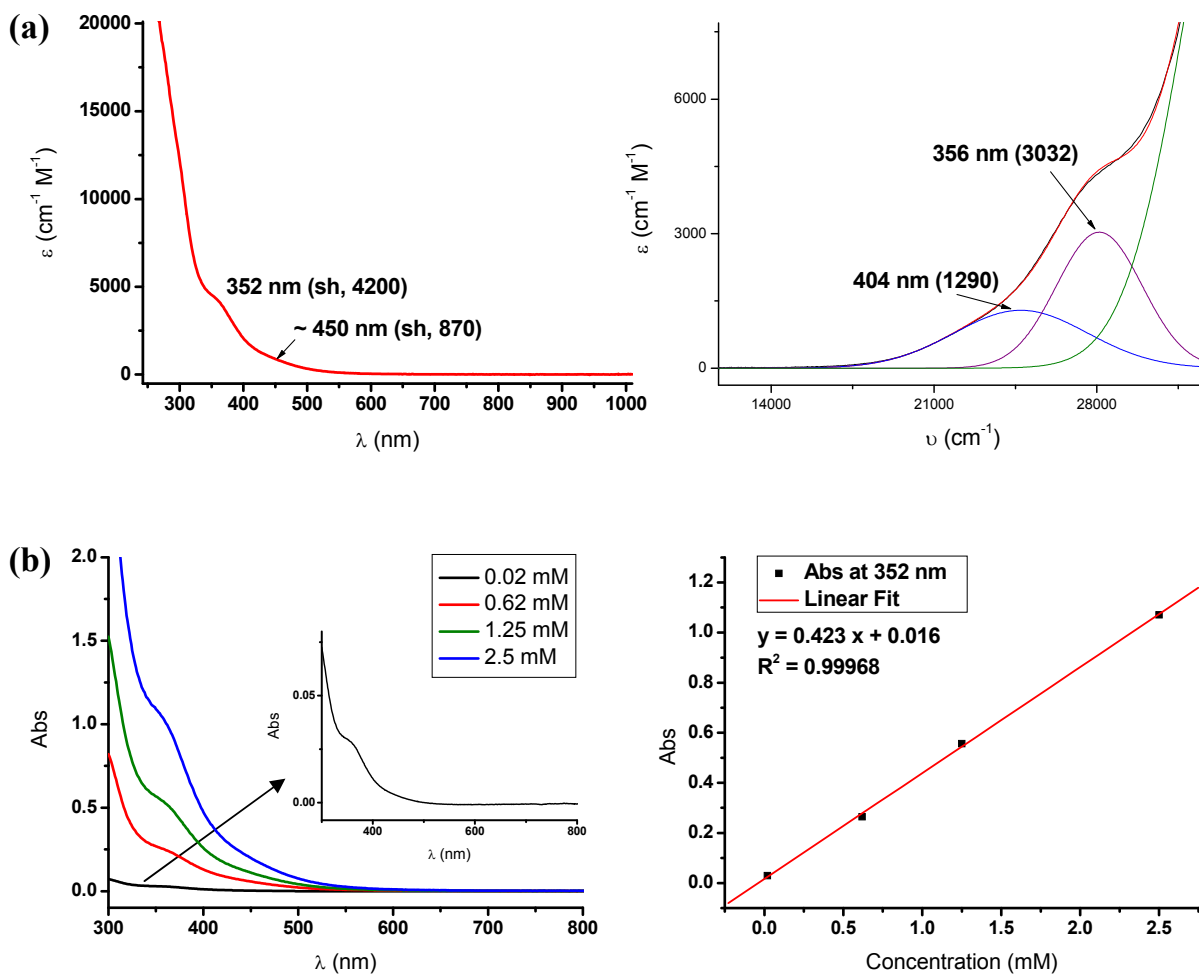


**Figure S12.** (a) UV-vis spectra and Gaussian fit of **2** in MeCN; (b) overlay of the UV-vis spectra at different concentrations (pathlength = 1.0 mm) and linear fit of the absorbance at 352 nm.

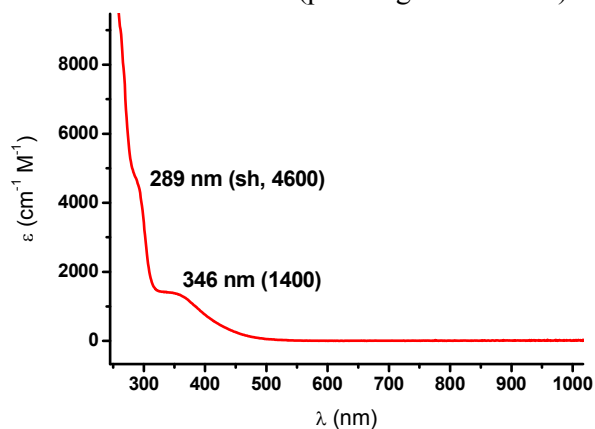


**Figure S13.** UV-vis spectrum and of **3** in MeCN.

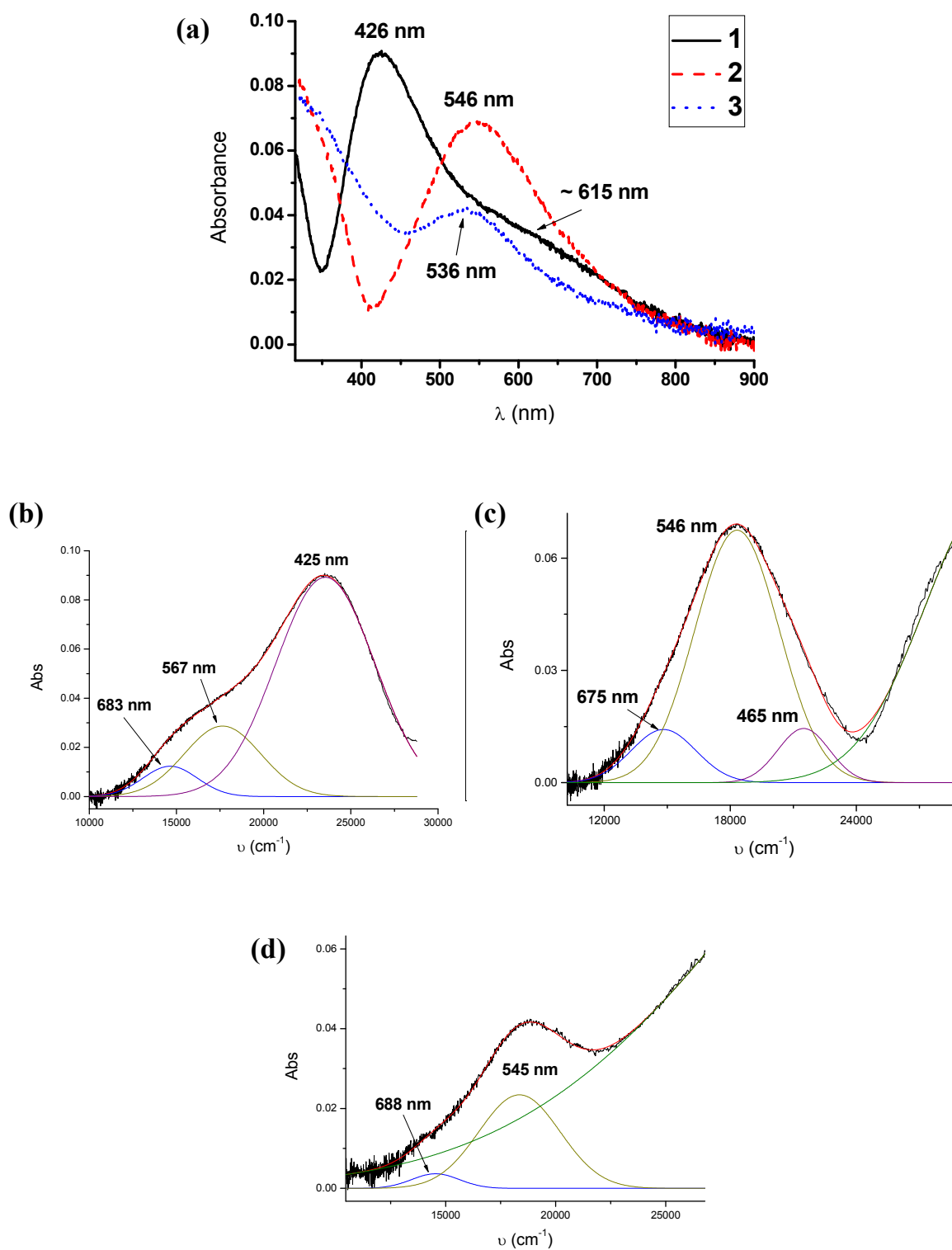


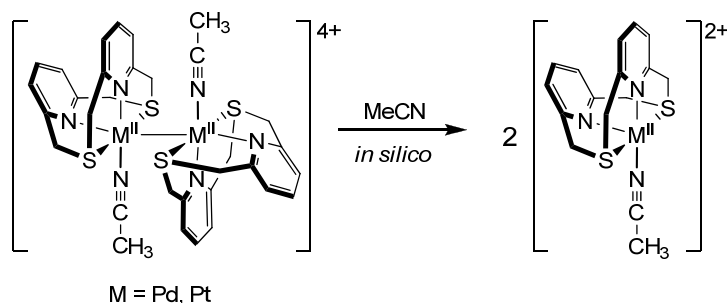
**Figure S14.** (a) Solid-state UV-vis spectra of **1**, **2** and **3**; Gaussian fits of **1** (b), **2** (c) and **3** (d).

## VII. Computational details

The density functional theory (DFT) calculations were performed with the program package Gaussian 09.<sup>4</sup> The B3LYP functional was employed,<sup>5</sup> the LANL2DZ basis set and Hay and Wadt effective core potentials were used for Pd and Pt,<sup>6</sup> and the 6-31G\* basis set was used for S, C, N, and H. Similar results have been obtained with the Stevens (CEP-31G)<sup>7</sup> valence basis set and effective core potential, which have been shown previously to reproduce well experimental parameters of Pd complexes.<sup>8</sup> Single point calculations were performed on the crystallographic coordinates of the cations of **1**, **2**, and **3**. The ground state wavefunctions were investigated by analysis of the frontier MOs (Tables S3 and S5), and the atomic contributions to MOs were calculated using the program Chemissian.<sup>9</sup> The Bond Analysis Tool in Chemissian was used to calculate the Mayer bond order indexes between atoms. TD-DFT calculations were employed to obtain the predicted absorption bands and their major contribution transitions (Tables S4 and S6). The calculated UV-vis spectrum was generated using Chemissian, with a full width at half maximum (FWHM) value of 3,500 cm<sup>-1</sup> (Figures S16 and S17).

### DFT calculations of the dissociation of **1** in MeCN

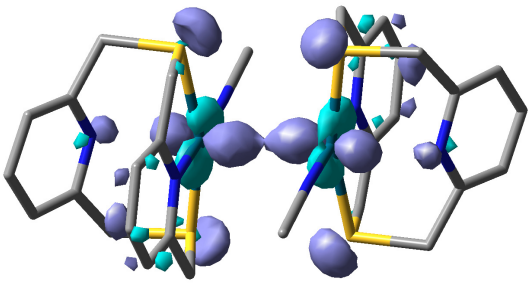
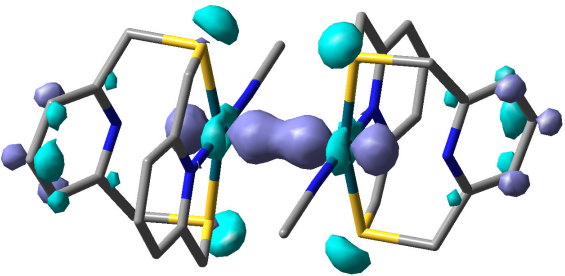
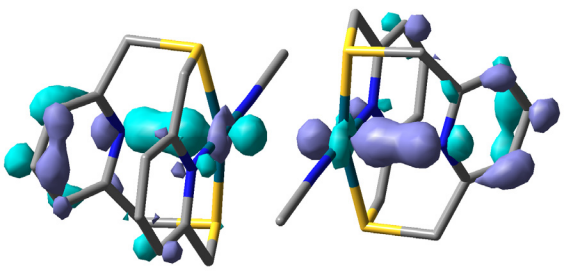
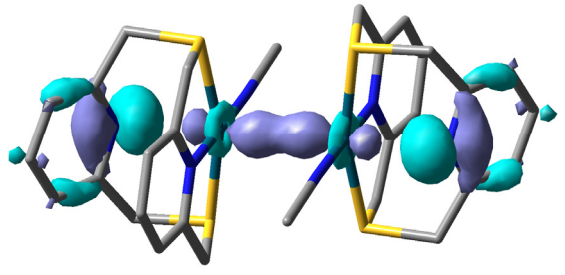
Geometry optimization calculations were performed using the functional/basis sets combination described above and the Polarizable Continuum Model solvation method.<sup>10</sup> Preliminary geometry optimizations of the cations of **1** and **2** in MeCN show that the dinuclear species dissociate during the optimization steps to give non-interacting mononuclear species. This behavior supports our hypothesis that **1** easily dissociates in MeCN into an asymmetric mononuclear species (Figure S15). More detailed computational studies on these systems will be reported elsewhere.



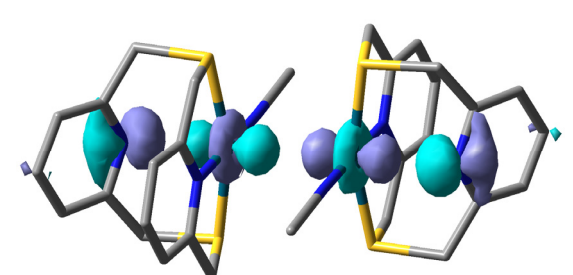
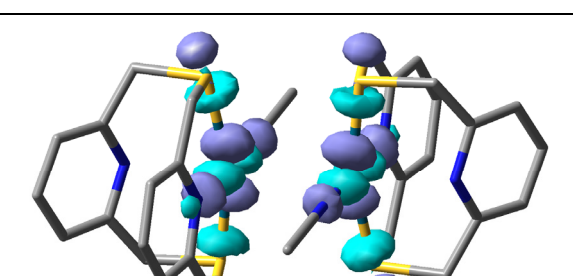
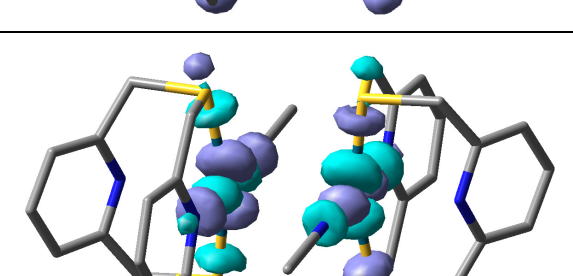
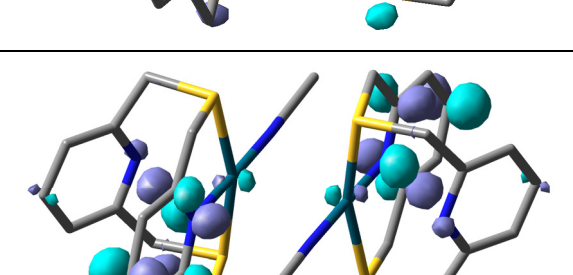
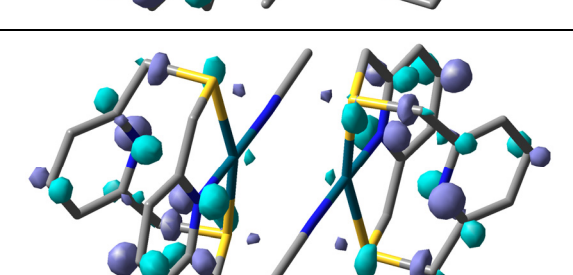
**Figure S15.** Observed *in silico* dissociation of the cation of **1** and **2** into mononuclear species in MeCN.

Electronic Supporting Information (ESI) for Chemical Communications  
 This journal is (c) The Royal Society of Chemistry 2011

**Table S3.** Isocontour plots and energies of selected molecular orbitals for **1**. The atomic Mulliken contributions to the MOs are shown for the Pd atoms (with d, p, and s orbital contribution), the equatorial pyridine N ( $N_{eq}$ ), the axial pyridine N ( $N_{ax}$ ), the MeCN (MeCN), and the S atoms (S). Balance contribution comes from ligand-based C atoms.

MO # Energy (eV)	Mos (0.05 isocontour value)	Pd (%)	$N_{eq}$ (%)	$N_{ax}$ (%)	MeCN (%)	S (%)
HOMO-21 161 -20.325		38 total: 34 4d 2 5p 2 5s	1	4	1	26
HOMO-13 169 -19.330		31 total: 22 4d 8 5s 1 5p	3	1	0	25
HOMO-10 172 -18.726		25 total: 20 4d 4 5s 1 5p	4	13	0	6
HOMO-3 179 -17.400		22 total: 14 4d 8 5p	1	46	0	3

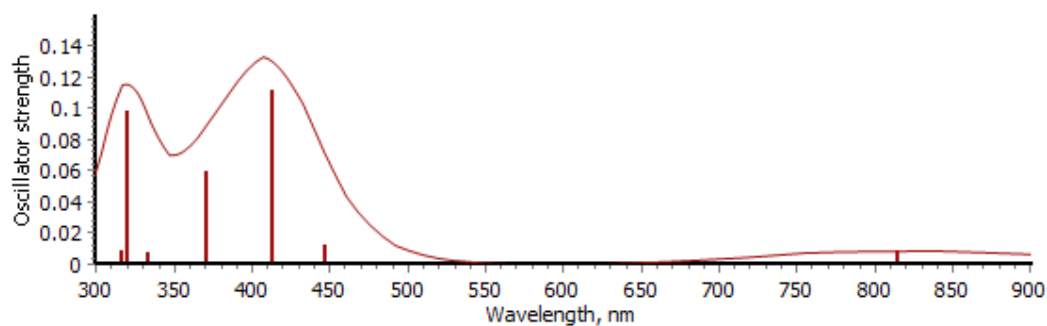
Electronic Supporting Information (ESI) for Chemical Communications  
 This journal is (c) The Royal Society of Chemistry 2011

HOMO 182 -16.526		43 total: 42 4d 1 5s	2	27	1	9
LUMO 183 -13.948		45 total: 42 4d 2 5s 1 5p	8	0	5	34
LUMO+1 184 -13.820		45 total: 44 4d 1 5s	10	0	6	31
LUMO+2 185 -12.842		8 total: 6 5p 2 4d	14	3	1	6
LUMO+4 187 -11.880		7 total: 7 5p	7	9	0	22

**Note:** The HOMO-10  $\sigma$ -bonding molecular orbital of **1** suggests a bonding interaction between the Pd center and the N atom of the axial pyridine. In addition, the calculated Pd-N<sub>axial</sub> bond order of 0.29 provides further support for this bonding interaction.

**Table S4.** TD-DFT calculated absorption bands and their composition for **1**. Only the transitions with oscillator strengths greater than 0.005 are shown; the major contributing transitions have more than 5% contribution to the absorption band.

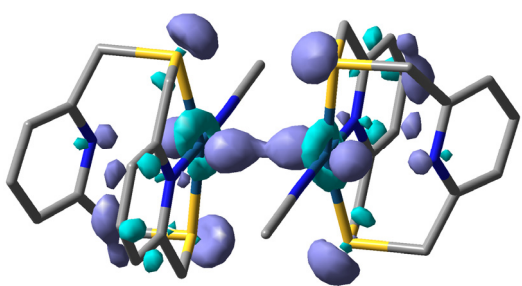
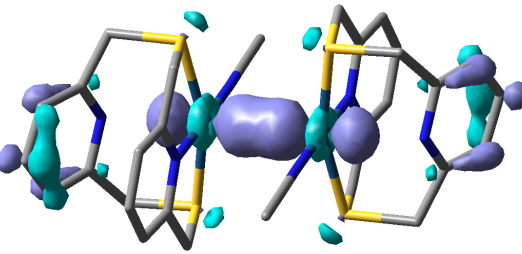
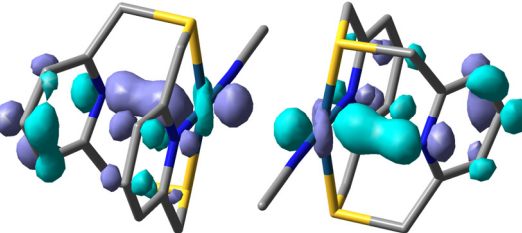
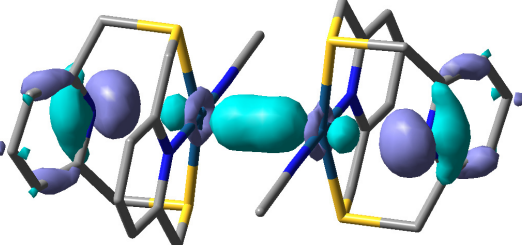
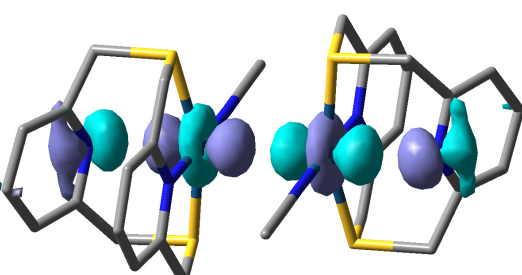
Wavelength (nm)	Oscillator strength	Major contributing transitions
814.8	0.008	HOMO → LUMO (92%), HOMO-3 → LUMO+1 (5%)
446.7	0.013	HOMO-1 → LUMO+1 (92%), HOMO → LUMO (5%)
413.0	0.111	HOMO → LUMO+2 (100%)
370.5	0.059	HOMO-6 → LUMO+1 (67%), HOMO-7 → LUMO (18%)
319.8	0.098	HOMO → LUMO+4 (93%)



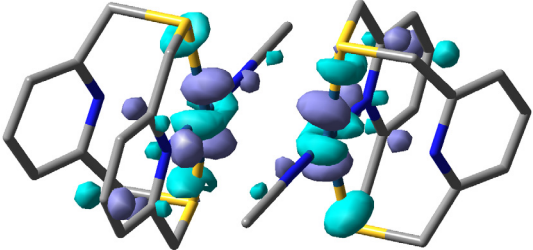
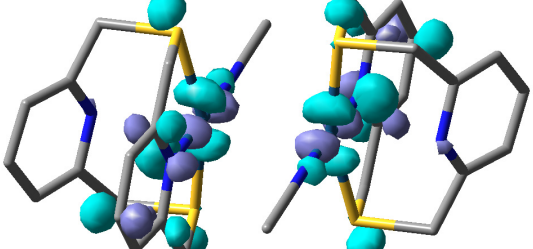
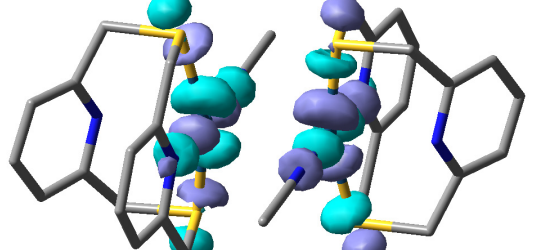
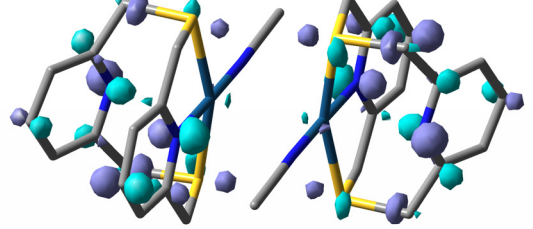
**Figure S16.** TD-DFT calculated UV-vis spectrum of **1**.



**Table S5.** Isocontour plots and energies of selected molecular orbitals for **2**. The atomic Mulliken contributions to the MOs are shown for the Pt atoms (with d, p, and s orbital contribution), the equatorial pyridine N ( $N_{eq}$ ), the axial pyridine N ( $N_{ax}$ ), the MeCN (MeCN), and the S atoms (S). Balance contribution comes from ligand-based C atoms.

MO # Energy (eV)	MOs (0.05 isocontour value)	Pt (%)	$N_{eq}$ (%)	$N_{ax}$ (%)	MeCN (%)	S (%)
HOMO-21 161 -20.272		30 total: 26 4d 2 5p 3 5s	3	4	0	28
HOMO-14 168 -19.475		42 total: 31 4d 10 5s 1 5p	1	1	0	16
HOMO-9 173 -18.613		27 total: 22 4d 4 5s 1 5p	5	13	0	1
HOMO-3 179 -17.335		23 total: 14 4d 9 5p	0	47	0	1
HOMO 182 -16.019		52 total: 50 4d 2 5s	1	22	1	8

Electronic Supporting Information (ESI) for Chemical Communications  
 This journal is (c) The Royal Society of Chemistry 2011

LUMO 183 -13.168		37 total: 26 4d 6 5p 5 5s	6	1	3	25
LUMO+1 184 -12.868		43 total: 42 4d 1 5s	8	0	3	34
LUMO+2 185 -12.839		15 total: 14 4d 1 5p	13	2	3	20
LUMO+4 187 -11.960		7 total: 6 5p 1 4d	8	9	0	22

**Note:** The HOMO-9  $\sigma$ -bonding molecular orbital of **2** suggests a bonding interaction between the Pt center and the N atom of the axial pyridine. In addition, the calculated Pt-N<sub>axial</sub> bond order of 0.29 provides further support for this bonding interaction.

**Table S6.** TD-DFT calculated absorption bands and their composition for **2**. Only the transitions with oscillator strengths greater than 0.005 are shown; the major contributing transitions have more than 5% contribution to the absorption band.

Wavelength (nm)	Oscillator strength	Major contributing transitions
637.5	0.047	HOMO → LUMO (82%), HOMO → LUMO+2 (14%)
504.7	0.094	HOMO → LUMO+2 (82%), HOMO → LUMO (16%)
373.2	0.133	HOMO → LUMO+4 (100%)
339.1	0.035	HOMO-3 → LUMO (100%)
307.4	0.042	HOMO-4 → LUMO+1 (56%), HOMO-7 → LUMO (21%), HOMO-1 → LUMO+1 (8%)

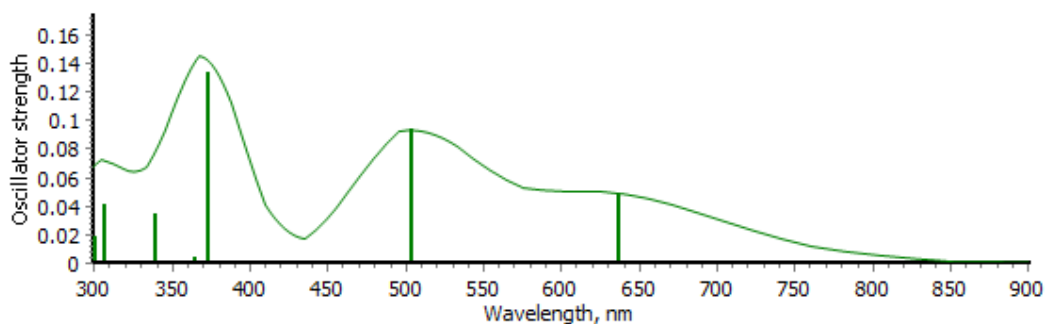


**Figure S17.** TD-DFT calculated UV-vis spectrum of **2**.

### Atoms in Molecules (AIM) Analysis of 1, 2, and 3

The Atoms in Molecules (AIM) method uses topological analysis of the electron distribution to characterize the bonding interactions.<sup>11</sup> The method was employed to characterize the nature of metal-metal and axial metal-pyridine interactions in **1**, **2**, and **3**. In all cases (3,-1) bond critical points were found along the bond path between the two interacting atoms, confirming the presence of bonding interactions. For these interactions, the ellipticity values were found to be between 0.04 and 0.11, suggesting the presence of  $\sigma$ -bonding interactions. Topological analyses of the electron density were performed using the XAIM program,<sup>12</sup> which located and characterized the critical points (Table S7).

**Table S7.** AIM analysis results for the metal-metal and metal-axial pyridine interactions in **1**, **2**, and **3**.

Compound	Interaction	Bond critical point	Ellipticity	Bonding type
<b>1</b>	Pd $\cdots$ Pd'	(3,-1)	0.10	$\sigma$ -bonding
	Pd $\cdots$ N2 <sub>axial</sub>	(3,-1)	0.05	$\sigma$ -bonding
<b>2</b>	Pt $\cdots$ Pt'	(3,-1)	0.11	$\sigma$ -bonding
	Pt $\cdots$ N2 <sub>axial</sub>	(3,-1)	0.06	$\sigma$ -bonding
<b>3</b>	Pd $\cdots$ Pd'	(3,-1)	0.04	$\sigma$ -bonding
	Pd $\cdots$ N2 <sub>axial</sub>	(3,-1)	0.08	$\sigma$ -bonding

### VIII. Reactivity studies of **3**.

**General experimental procedure.** All operations were performed in a nitrogen-filled glovebox. An NMR tube capped with a rubber septum was charged with a solution of [(N2S2)Pd<sup>II</sup>Me]<sub>2</sub>(OTf)<sub>2</sub> (2.0 mg, 1.8 μmol) in 1.0 mL acetone-*d*<sub>6</sub>. A solution of 2 equiv. (Cp<sub>2</sub>Fe)PF<sub>6</sub> (Fc<sup>+</sup>) in 1.4 mL of acetone-*d*<sub>6</sub> was added in portions with a microsyringe and the mixture was thoroughly mixed after each addition. Dioxane standard was added with a microsyringe when the mixture has stopped reacting based on <sup>1</sup>H NMR.

**Table S8.** Yields<sup>a</sup> of products from the reaction of **3** with 2 equiv Fc<sup>+</sup> in acetone-*d*<sub>6</sub>.

Reaction Time	[(N2S2)Pd <sup>IV</sup> Me <sub>2</sub> ] <sup>2+</sup>	[(N2S2)Pd <sup>II</sup> ] <sup>2+</sup> species	Unreacted <b>3</b>
5 min	21%	24%	55%
1 h	32%	39%	29%
3 h	36%	41%	22%
8 h	40%	43%	17%
23 h	44% (46% <sup>b</sup> )	41%	15% (13% <sup>b</sup> )

<sup>a</sup>Reported yields are relative yields (unless specified). <sup>b</sup>Absolute yield vs. dioxane as internal standard.

#### Notes:

1. The identity of [(N2S2)Pd<sup>IV</sup>Me<sub>2</sub>]<sup>2+</sup> was confirmed by independent synthesis (to be reported elsewhere). <sup>1</sup>H NMR (acetone-*d*<sub>6</sub>, 300 MHz), δ (ppm): 2.61 (s, 6H, Pd-CH<sub>3</sub>), 5.66 (d, *J* = 18 Hz, 4H, CH<sub>2</sub>), 5.96 (d, *J* = 18 Hz, 4H, CH<sub>2</sub>), 7.79 (d, *J* = 8.1 Hz, 4H, Py H<sub>meta</sub>), 8.11 (t, *J* = 8.0 Hz, 2H, Py H<sub>para</sub>). This species was also identified by ESI-MS of the reaction solution (*m/z* found 205.0063, calculated for [(N2S2)Pd<sup>IV</sup>Me<sub>2</sub>]<sup>2+</sup>: 205.0051). The [(N2S2)Pd<sup>II</sup>]<sup>2+</sup> species is most likely an acetone adduct, as its NMR chemical shifts are similar to those for **1** dissolved in acetone-*d*<sub>6</sub>.
2. The relative yields of [(N2S2)Pd<sup>IV</sup>Me<sub>2</sub>]<sup>2+</sup> and unreacted **3** were obtained by the integration of the corresponding methyl groups assuming that there are no loss of methyl group in any side reactions; the relative yields of [(N2S2)Pd<sup>II</sup>]<sup>2+</sup> species were calculated by subtracting the integration of CH<sub>2</sub> groups of [(N2S2)Pd<sup>IV</sup>Me<sub>2</sub>]<sup>2+</sup> and unreacted **3** from the total integration in the CH<sub>2</sub> region.
3. Similar yields were obtained in CD<sub>3</sub>CN, although the reaction was slightly slower and the NMR of the reaction mixture was difficult to integrate accurately, likely due to formation of asymmetric Pd-solvento complexes. This provides evidence that **3** dissociates in MeCN and the dinuclear structure is needed for an efficient methyl group transfer.

Electronic Supporting Information (ESI) for Chemical Communications  
This journal is (c) The Royal Society of Chemistry 2011

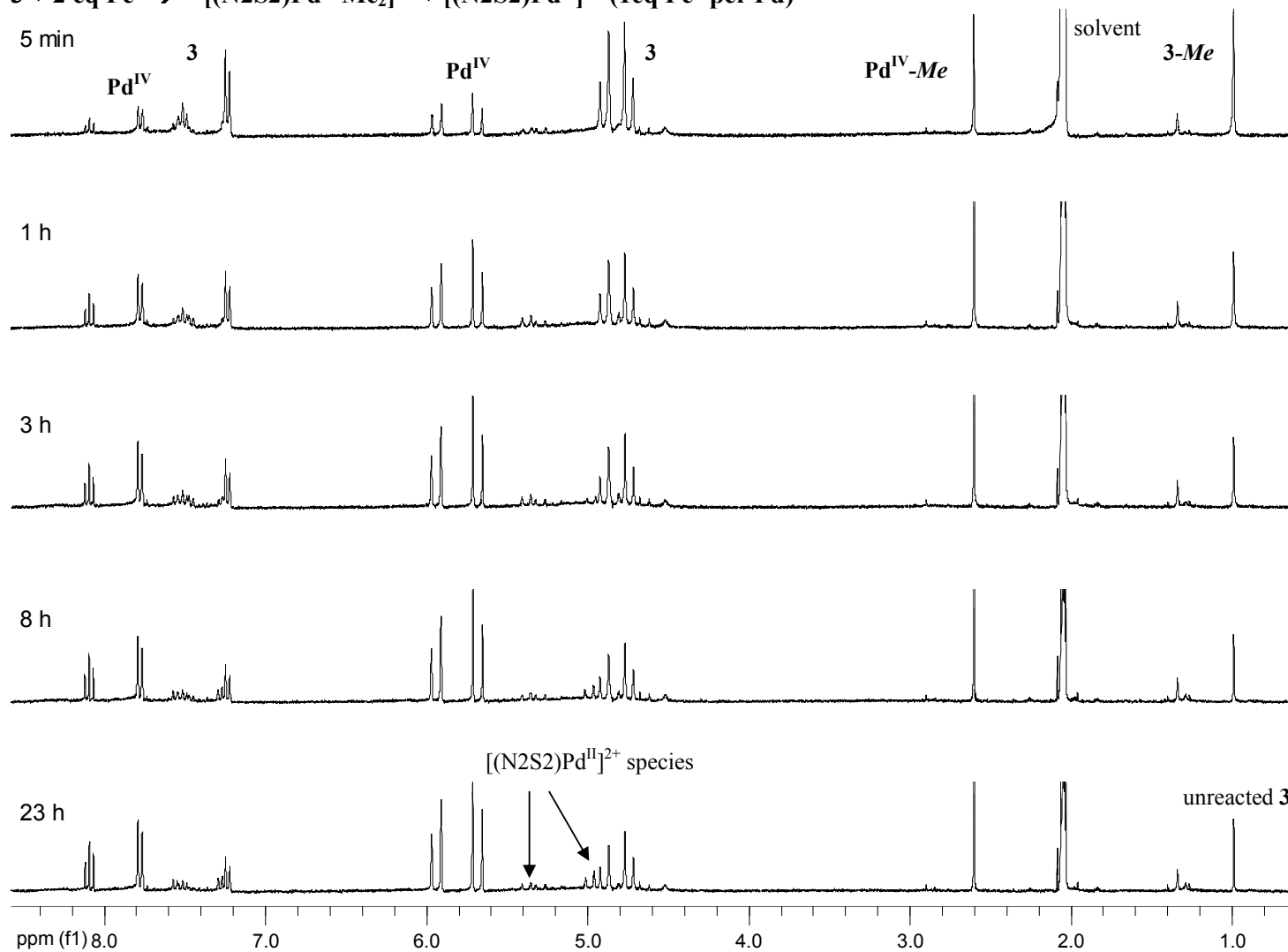
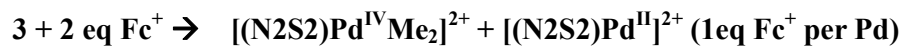


**Figure S18.**  $^1\text{H}$  NMR spectra of **3** reacted with 2 equiv  $\text{Fc}^+$  in acetone- $d_6$  at different time points.

## IX. References

1. a) E. C. Constable, A. C. King, P. R. Raithby, *Polyhedron*, 1998, **17**, 4275; b) E. C. Constable, J. Lewis, V. E. Marquez, P. R. Raithby, *J. Chem. Soc., Dalton Trans.*, 1986, 1747.
2. T. Moriguchi, S. Kitamura, K. Sakata, A. Tsuge, *Polyhedron*, 2001, **20**, 2315.
3. R. E. Rulke, J. M. Ernsting, A. L. Spek, C. J. Elsevier, P. W. N. M. v. Leeuwen, K. Vrieze, *Inorg. Chem.*, 1993, **32**, 5769.
4. M. J. T. Frisch, G. W.; Schlegel, H. B.; Scuseria, G. E.; Robb, M. A.; Cheeseman, J. R.; Montgomery, Jr., J. A.; Vreven, T.; Kudin, K. N.; Burant, J. C.; Millam, J. M.; Iyengar, S. S.; Tomasi, J.; Barone, V.; Mennucci, B.; Cossi, M.; Scalmani, G.; Rega, N.; Petersson, G. A.; Nakatsuji, H.; Hada, M.; Ehara, M.; Toyota, K.; Fukuda, R.; Hasegawa, J.; Ishida, M.; Nakajima, T.; Honda, Y.; Kitao, O.; Nakai, H.; Klene, M.; Li, X.; Knox, J. E.; Hratchian, H. P.; Cross, J. B.; Bakken, V.; Adamo, C.; Jaramillo, J.; Gomperts, R.; Stratmann, R. E.; Yazyev, O.; Austin, A. J.; Cammi, R.; Pomelli, C.; Ochterski, J. W.; Ayala, P. Y.; Morokuma, K.; Voth, G. A.; Salvador, P.; Dannenberg, J. J.; Zakrzewski, V. G.; Dapprich, S.; Daniels, A. D.; Strain, M. C.; Farkas, O.; Malick, D. K.; Rabuck, A. D.; Raghavachari, K.; Foresman, J. B.; Ortiz, J. V.; Cui, Q.; Baboul, A. G.; Clifford, S.; Cioslowski, J.; Stefanov, B. B.; Liu, G.; Liashenko, A.; Piskorz, P.; Komaromi, I.; Martin, R. L.; Fox, D. J.; Keith, T.; Al-Laham, M. A.; Peng, C. Y.; Nanayakkara, A.; Challacombe, M.; Gill, P. M. W.; Johnson, B.; Chen, W.; Wong, M. W.; Gonzalez, C.; and Pople, J. A., *Gaussian 03, revision C.02*, Gaussian, Inc., Wallingford CT, 2004; a) G. W. T. M. J. Frisch, H. B. Schlegel, G. E. Scuseria, M. A. Robb, J. R. Cheeseman, G. Scalmani, V. Barone, B. Mennucci, G. A. Petersson, H. Nakatsuji, M. Caricato, X. Li, H. P. Hratchian, A. F. Izmaylov, J. Bloino, G. Zheng, J. L. Sonnenberg, M. Hada, M. Ehara, K. Toyota, R. Fukuda, J. Hasegawa, M. Ishida, T. Nakajima, Y. Honda, O. Kitao, H. Nakai, T. Vreven, J. A. Montgomery, Jr., J. E. Peralta, F. Ogliaro, M. Bearpark, J. J. Heyd, E. Brothers, K. N. Kudin, V. N. Staroverov, R. Kobayashi, J. Normand, K. Raghavachari, A. Rendell, J. C. Burant, S. S. Iyengar, J. Tomasi, M. Cossi, N. Rega, J. M. Millam, M. Klene, J. E. Knox, J. B. Cross, V. Bakken, C. Adamo, J. Jaramillo, R. Gomperts, R. E. Stratmann, O. Yazyev, A. J. Austin, R. Cammi, C. Pomelli, J. W. Ochterski, R. L. Martin, K. Morokuma, V. G. Zakrzewski, G. A. Voth, P. Salvador, J. J. Dannenberg, S. Dapprich, A. D. Daniels, O. Farkas, J. B. Foresman, J. V. Ortiz, J. Cioslowski, D. J. Fox., *Gaussian 09, Revision A.02*, Gaussian, Inc., Wallingford CT, 2009.
5. a) A. D. Becke, *J. Chem. Phys.*, 1993, **98**, 1372; b) C. T. Lee, W. T. Yang, R. G. Parr, *Phys. Rev. B*, 1988, **37**, 785.
6. a) P. J. Hay, W. R. Wadt, *J. Chem. Phys.*, 1985, **82**, 270; b) P. J. Hay, W. R. Wadt, *J. Chem. Phys.*, 1985, **82**, 299.

Electronic Supporting Information (ESI) for Chemical Communications  
This journal is (c) The Royal Society of Chemistry 2011

---

7. a) W. J. Stevens, H. Basch, M. Krauss, *J. Chem. Phys.*, 1984, **81**, 6026; b) W. J. Stevens, M. Krauss, H. Basch, P. G. Jasien, *Can. J. Chem.*, 1992, **70**, 612.
8. a) N. A. Foley, M. Lail, J. P. Lee, T. B. Gunnoe, T. R. Cundari, J. L. Petersen, *J. Am. Chem. Soc.*, 2007, **129**, 6765; b) A. S. Veige, L. M. Slaughter, P. T. Wolczanski, N. Matsunaga, S. A. Decker, T. R. Cundari, *J. Am. Chem. Soc.*, 2001, **123**, 6419.
9. L. Skripnikov, *Chemissian, version 1.771*, 2010, [www.chemissian.com](http://www.chemissian.com) (accessed June 2011).
10. J. Tomasi, B. Mennucci, R. Cammi, *Chem. Rev.*, 2005, **105**, 2999.
11. a) R. F. W. Bader, *Chem. Rev.*, 1991, **91**, 893; b) R. F. W. Bader, *Atoms in Molecules: A Quantum Theory*, Oxford University Press, New York, 1994.
12. J. C. O. Alba, C. B. Jane, *XAIM*, Universitat Rovira i Virgili, Tarragona, Spain, 1998, <http://www.quimica.urv.es/XAIM/> (accessed August 2011).